Nucleation and Growth of Insulin Fibrils in Bulk Solution and at Hydrophobic Polystyrene Surfaces

M. I. Smith,* J. S. Sharp,* and C. J. Roberts†

*School of Physics and Astronomy and Nottingham Nanotechnology and Nanoscience Centre, and †Laboratory of Biophysics and Surface Analysis, School of Pharmacy, and Nottingham Nanotechnology and Nanoscience Centre, The University of Nottingham, Nottingham, NG7 2RD, United Kingdom

ABSTRACT A technique was developed for studying the nucleation and growth of fibrillar protein aggregates. Fourier transform infrared and attenuated total reflection spectroscopy were used to measure changes in the intermolecular β-sheet content of bovine pancreatic insulin in bulk solution and on model polystyrene (PS) surfaces at pH 1. The kinetics of β-sheet formation were shown to evolve in two stages. Combined Fourier transform infrared, dynamic light scattering, atomic force microscopy, and thioflavin-T fluorescence measurements confirmed that the first stage in the kinetics was related to the formation of nonfibrillar aggregates that have a radius of 13 ± 1 nm. The second stage was found to be associated with the growth of insulin fibrils. The β-sheet kinetics in this second stage were used to determine the nucleation and growth rates of fibrils over a range of temperatures between 60°C and 80°C. The nucleation and growth rates were shown to display Arrhenius kinetics, and the associated energy barriers were extracted for fibrils formed in bulk solution and at PS surfaces. These experiments showed that fibrils are nucleated more quickly in the presence of hydrophobic PS surfaces but that the corresponding fibril growth rates decrease. These observations are interpreted in terms of the differences in the attempt frequencies and energy barriers associated with the nucleation and growth of fibrils. They are also discussed in the context of differences in protein concentration, mobility, and conformational and colloidal stability that exist between insulin molecules in bulk solution and those that are localized at hydrophobic PS interfaces.

INTRODUCTION

The effects of surfaces and interfaces on the misfolding and subsequent aggregation of proteins are an important consideration in a number of biological and technologically important areas. For example the presence of an abundance of interfaces in vivo has resulted in a number of studies that were designed to assess the role played by model biological membranes and synthetic surfaces on the stability and aggregation properties of proteins (1–4). These separate studies showed that the presence of surfaces and interfaces can have a profound effect on aggregate development and that the growth rates and final aggregate morphologies are sensitive to the details of the surface chemistry of an interface (e.g., hydrophobicity, charge). However, many of these studies are semiquantitative in nature, and a more quantitative measure of the effects of surfaces and interfaces on the stability of proteins remains to be obtained.

Interfacial effects are particularly important for a number of protein conformational disease–related states that involve the aggregation of protein molecules into long fibrous structures called amyloid fibrils. These structures typically comprise linear aggregates of smaller protein units (e.g., monomers and dimers). They have diameters that are comparable to the dimensions of one or two protein molecules and can be many micrometers in length. These structures and their precursors have been linked to a number of diseases such as Alzheimer's disease, Huntington's disease, Parkinson's disease, type II diabetes, and Creutzfeldt-Jakob disease (5–8). In each case, the aggregates that are formed from different proteins have been found to exhibit very similar morphologies and to contain large amounts of chain-folded intermolecular β-sheet structures. This has recently led to the conclusion that amyloid fibril formation is a generic property of proteins (5–8). As a result, a significant amount of research has been carried out to try to develop an understanding of the molecular-level processes that result in their formation. The fact that these structures are usually formed in the presence of a wide range of biological interfaces also suggests that developing a greater knowledge of how protein/surface interactions affect the formation of these structures could help us to understand these processes.

Recent developments in the rapidly emerging field of nanotechnology also raise some important questions about the effects of surfaces and interfaces on the stability and aggregation properties of proteins and other biological macromolecules (9). Nanoscale materials and particles such as those being used in novel biosensing applications (10), immunological assays, and early gene gun–based delivery methods (11) have surface-to-volume ratios that are up to 10^8 times larger than bulk samples of the same materials. The surface-related effects that have already been reported in studies of protein aggregation (1–3) therefore have important

Submitted January 26, 2007, and accepted for publication May 8, 2007.

Address reprint requests to J. S. Sharp, School of Physics and Astronomy and Nottingham Nanotechnology and Nanoscience Centre, The University of Nottingham, Nottingham, NG7 2RD, UK. E-mail: james.sharp@nottingham.ac.uk.

Editor: Ruth Nussinov.

0006-3495/07/09/2143/09 $2.00

doi: 10.1529/biophysj.107.105338

implications for the nanotoxicology of a wide range of materials.

Protein aggregation is also of considerable interest to the pharmaceutical industry, where maintaining the stability of proteins at low pH is vital during the production and purification of protein-based drugs such as insulin (12–14). The storage of proteins is also an important factor in determining the shelf life of these materials. In particular, the effects of storing and processing proteins such as insulin in different containers are likely to affect their long-term stability.

In this article we describe an experimental study of aggregation and amyloid fibril formation in bovine pancreatic insulin (BPI) at elevated temperatures and low pH. Fourier transform infrared (FTIR) spectroscopy and attenuated total reflection (ATR) spectroscopy are used to monitor the aggregation/β-sheet-formation kinetics of this protein in bulk solution and on model hydrophobic polystyrene (PS) surfaces. The temperature dependence of the nucleation/lag times and aggregation rates associated with insulin fibril formation are used to determine the energy barriers associated with the nucleation and growth of these structures, respectively. Complementary techniques such as atomic force microscopy (AFM), dynamic light scattering (DLS), and thioflavin-T fluorescence assays were also used to monitor the growth of the protein aggregates. To the best of our knowledge, these experiments represent the first quantitative study of the effects of surfaces and interfaces on the aggregation properties of proteins.

EXPERIMENTAL PROCEDURES

Stock solutions of 0.025M NaCl and 0.1 M HCl (pH 1) were prepared in preboiled deuterium oxide (D_2O, Goss Scientific, Essex, UK). These solutions were then sealed in 15-ml sample vials and degassed by being placed in a water bath at ~85°C for 1 h. The solutions were then allowed to cool to room temperature. BPI (Sigma Aldrich, Gillingham, UK, mol wt = 5733, catalog No. I5500) was then dissolved in the solutions at a concentration of 20 mg·ml^{-1} (~3.5 mM). A single batch of BPI was used in all the experiments described below because batch-to-batch variations in the properties of insulin have been reported (15). The resulting protein solutions were then left at room temperature in sealed vials for a further 24 h to enable the complete hydrogen-deuterium exchange of labile hydrogens on the insulin molecules.

Fourier transform infrared spectroscopy

FTIR spectroscopy measurements were collected using a Varian FTS40 Pro spectrometer equipped with Resolutions Pro 4.0 software. Each averaged spectrum was collected using a spectral resolution of 4 cm^{-1}, and the time between the collection of the averaged spectra was 15 s. Deuterium oxide was used as the solvent in these experiments to avoid difficulties associated with the overlap of liquid water peaks with the amide I and amide II regions of the protein IR spectra. No spectral subtraction was performed on the infrared spectra. However, the baseline of the spectra tilted during the experiments as a result of variations in the intensity of the IR light source used in the spectrometer. This tilting was corrected for by subtracting a linear baseline, which was calculated using the flat regions of the spectra in the ranges 850–1100 cm^{-1} and 1750–2100 cm^{-1}.

Bulk solution IR spectroscopy measurements were performed over a range of temperatures from 60°C to 80°C using an electrically heated liquid transmission cell with zinc selenide (ZnSe) windows (Specac, Orpington, UK). One of the ZnSe windows was predrilled with two holes through its larger faces to allow the cell volume to be exchanged with fluid. Before the experiments, one side of each ZnSe window was spin coated with a 2 wt % solution of PS (M_w = 600 kDa, M_w/M_n = 1.09, Polymer Source) in toluene (spin speed 2500 rpm) and then annealed under vacuum at ~120°C to remove residual solvent. This resulted in the formation of an ~200-nm-thick PS film (as measured using atomic force microscopy). This was done to protect the windows from the acidic solutions used in the experiments. Acidic solutions are known to dissolve ZnSe, and Zn^{2+} ions have been shown to promote the onset of fibril formation in some proteins (16).

The two ZnSe windows were then placed together with their PS-coated surfaces separated by a 75-μm-thick poly (tetrafluoroethylene) (PTFE) spacer. This procedure was used to produce a small cavity with a 75-μm-thick path length for performing liquid transmission IR studies. The resulting assembly was then sealed around the edge using a highly viscous solution of PS in toluene. The windows and spacer were then annealed at ~100°C for 2 h to remove residual toluene and to seal the edges of the cell so that it would not leak when filled. The window assembly was then placed in the sample cell and loaded into the sample chamber of the FTIR spectrometer. Stainless steel tubing was then attached to the sample cell so that the volume of the cell could be exchanged from outside the FTIR sample chamber. The chamber was then purged with dry air.

The fully assembled liquid cell was then heated to the desired experimental temperature, which was monitored using a precalibrated t-type thermocouple buried in the metal body of the cell (close to the ZnSe windows). Deuterium oxide–based stock solution was then injected into the cell. A background spectrum was collected by averaging 100 individual spectra, and the stock solution was replaced with an identical solution containing 20 mg·ml^{-1} of BPI. Immediately after the injection of the protein solution, spectra were collected with a time resolution of 15 s. In each case 15 spectral scans were averaged per spectrum. All spectra were then ratioed to the spectrum obtained from the D_2O stock solution.

FTIR spectra of BPI adsorbed at PS surfaces were also collected using an ATR liquid cell (Specac). The ATR geometry uses the total internal reflection of IR radiation at a ZnSe/solution interface to produce an evanescent field that penetrates ~1 μm into the solution. Because the intensity of this field decays exponentially as a function of distance, the IR spectra that are obtained using this technique are extremely sensitive to material that is close to the interface.

Thin films (~200 nm) of PS were spin coated onto one side of a ZnSe ATR crystal using the same experimental parameters used to coat the ZnSe windows described above. The PS coated crystal was then annealed under vacuum at ~120°C to remove residual solvent and then allowed to cool to room temperature. The ATR crystal was then loaded into the ATR liquid cell and heated to the required temperature using a circulating water bath. The temperature in the cell was monitored using a thermocouple embedded in the ATR cell top plate that had been precalibrated against the measured temperature inside the cell. The sample cell was then filled with the D_2O-based stock solution and allowed to equilibrate before a background spectrum was collected by averaging 100 individual spectra. The solution was then replaced with an identical solution containing 20 mg·ml^{-1} BPI, and spectra were collected every 15 s (averaging 15 scans per spectrum).

Atomic force microscopy of BPI aggregates

BPI was dissolved in the D_2O-based stock solutions at a concentration of 20 mg·ml^{-1}. Bulk solution insulin fibrils were formed by incubating sealed vials of the resulting protein solution in a water bath at 60°C. The vials were then removed at regular time intervals and placed in an ice bucket to slow down the fibril growth rates and quench in the structure of the fibrils.

Surface-adsorbed fibrils were prepared on PS-coated single-crystal silicon wafers (Si, Compart Technology, [100], ~300 μm thick). An ~200-nm-thick PS film was spin coated on to the Si wafers from a 2 wt % solution in toluene and annealed at 120°C under vacuum. The resulting PS

films were then submerged (facing downward) in vials containing similar solutions to those used to form the bulk fibrils and were incubated in a water bath at 60°C. The sealed vials were then removed at regular time intervals and quenched in a bucket of ice.

In the case of the bulk solution fibrils, a droplet of each protein solution was transferred onto a clean PS-coated Si wafer and allowed to dry before being imaged with an Asylum Research MFP-3D AFM. The fibrils formed on the PS surfaces were simply allowed to dry out before being imaged. All samples were imaged using tapping-mode AFM.

Dynamic light-scattering studies

The time evolution of the average aggregate size in 20 mg·ml^{-1} solutions of BPI in D_2O-based stock solutions was studied at a temperature of 60°C using a Malvern Instruments DLS (4700 PCS).

Thioflavin-T studies

Thioflavin-T (ThT) fluorescence studies were used to monitor the kinetics of β-sheet formation during aggregation/fibril formation in BPI. Solutions of BPI (20 mg·ml^{-1}) containing ~2.5 μM ThT were placed on a glass coverslip inside an ~10-mm-diameter O-ring. A second coverslip was clamped on top of the O-ring to create a sealed sample cell. The cell was then placed on top of a home-made heater and mounted on the stage of an Olympus BX51 optical microscope equipped with fluorescence capabilities and a DP70 CCD camera and connected to a PC running Image Pro Plus software (Media Cybernetics). The protein solution was heated to 60°C, and the excited fluorescence measured through a filter ($\lambda \approx$ 470–490 nm, U-MNB2, Olympus) using the CCD camera. Optical micrographs of the solution in the sample cell were then collected at 30-s intervals. The Image Pro Plus software was then used to determine the average fluorescence intensity obtained from the optical micrographs as a function of time.

RESULTS AND DISCUSSION

Fig. 1 shows an example of a typical FTIR spectrum of the amide I and II regions that was obtained using the bulk liquid transmission cell. Spectra obtained from both the bulk liquid transmission cell and the ATR cell had similar features. Minor differences in the spectra were attributed to the wavenumber dependence of the penetration depth of the evanescent field in the ATR experiments. The spectra obtained for the combined amide I and II regions were fitted to five Lorentzian peaks (shown as the gray lines in Fig. 1) using a nonlinear least-squares fitting algorithm. The assignments of these peaks are given in the inset of Fig. 1. The sum of all these peaks is shown as the black solid line in the main panel of Fig. 1. The assignments of the peaks in the amide I region are consistent with literature reports of the positions of peaks that correspond to features associated with β-sheet, random coil, and α-helix (17–19). The two peaks used to represent the amide II region in our fitting procedure do not have any specific assignments and were simply used to describe the shape of the spectra. The shape of this region did not change during the course of the FTIR experiments, and these peaks were found to represent the shape of the amide II region accurately (see Fig. 1).

The small peak shown at ~1525 cm^{-1} in Fig. 1 forms part of the amide II region. As a result, this small feature was found to change in proportion to the other peaks in the amide

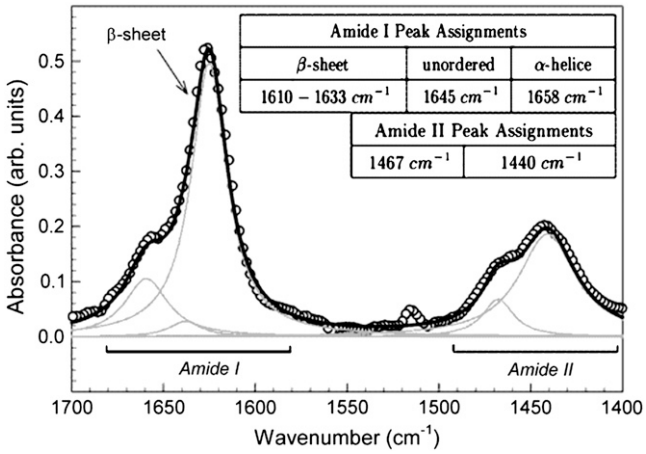

FIGURE 1 Infrared spectrum of the amide I and II spectral regions for bovine pancreatic insulin collected at 60°C and pH 1 after incubation for ~100 min. The gray lines show the five Lorentzian peaks that were used to fit the data (○). The inset shows a table of the peaks used to fit the data along with their protein structural assignments (17). The black solid line is the combined fit to the data and is given by summing the contributions of the five separate Lorentzian peaks.

II region during the FTIR experiments. This peak was not fitted because it would have involved introducing three additional parameters into the fitting procedure described above. The addition of a fitted peak at ~1525 cm^{-1} does not significantly affect the heights, positions, or widths of the other fitted peaks. Because of this, the smaller peak was ignored to speed up the optimization of the fitting process.

The fitting procedure was performed on all the spectra collected from each FTIR experiment. The positions of all but the β-sheet peak (1610–1633 cm^{-1}) were constrained to within $\pm$ 2 cm^{-1}, and the widths were constrained to within $\pm$ 5 cm^{-1}. The position of the β-sheet peak was allowed to vary by $\pm$12 cm^{-1} as reports by Nielsen and co-workers suggest that the position of this peak changes during the aggregation of insulin (17). The amplitudes of all the peaks were not constrained and were allowed to vary during the fitting procedure.

The fitting procedure typically gave an initial value for the ratio of the areas of the fitted peaks of 7%:54%:39% (β-sheet/α-helix/random coil). The final value of this ratio was typically found to be 76%:20%:4%. These values are in agreement with results obtained from other studies of insulin aggregation (17,19,20).

The areas of the peaks obtained from the fitting procedure were then used to generate plots of the kinetics of β-sheet growth, similar to those shown in Fig. 2. To decouple the effects of changes in the β-sheet content of the BPI molecules from effects caused by changing amounts of protein in the beam path, the area of the β-sheet peak was divided by the sum of the areas of the two peaks used to fit the amide II region in the same FTIR spectrum (see Fig. 1). The shape of the amide II region did not change during the experiments, indicating that this peak was insensitive to structural changes

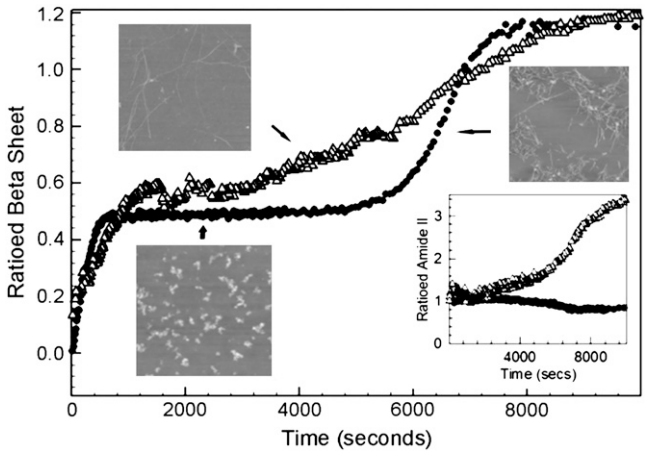

FIGURE 2 Kinetics of β-sheet formation during the aggregation of bovine pancreatic insulin. Data are shown for insulin aggregating in bulk solution (●) and near a PS surface (Δ). In both cases, the area of the β-sheet peak was divided by the total area of the amide II region collected at each time. The inset shows a plot of the variation in the area of the amide II region with time. In both cases, the area of this peak was divided by the initial area of this region. All data were collected at a temperature of 60°C and at pH 1. The AFM images shown as insets were collected using a scan area of 5 μm × 5 μm and show typical images of the observed aggregate morphologies at the times indicated by the solid arrows.

in the BPI molecules. This result is consistent with the results obtained by Hiramatsu and Kitagawa (21). The effects of hydrogen-deuterium (H-D) exchange on changes in the size and shape of the amide II region can be excluded as the bending mode of N-D (centered 1445 cm^{-1}) and N-H (centered 1545 cm^{-1}) are in very different places and are easily distinguishable using the FTIR technique. As described in the experimental section, the protein was initially placed in D_2O-based stock solutions for 24 h to facilitate the exchange of hydrogen atoms on the outside of the insulin molecules. The remaining hydrogen atoms buried in the center of the protein (14) were observed to undergo H/D exchange via a shift in the peak at 1545 cm^{-1} to 1445 cm^{-1}. However, in the case of the 60°C data, this change occurred over a period of time corresponding to the time taken to collect the first two FTIR spectra. This indicates that any residual H-D exchange occurs rapidly even at the lowest temperatures studied. This is confirmed by the results of similar studies performed by Dzwolak and co-workers (22,23). The amide II peak was therefore used as a measure of the amount of protein in the beam path. Dividing the area of the β-sheet peak by the area of each spectrum's amide II region in this way therefore gives a measure of the extent of β-sheet formation per unit mass of protein during aggregation/fibril formation.

As shown in the inset of Fig. 2, the total area of the amide II peak increases with time during the ATR experiments on PS surfaces. This increase was attributed to changes in the amount of insulin at the PS/water interface caused by the continued adsorption and aggregation of insulin at the PS surfaces. The area of the amide II peak measured in the bulk transmission cell experiments did not change appreciably during the course of the experiments. This is to be expected because the amount of protein in the IR beam path remains constant during these experiments.

Fig. 2 shows that the β-sheet kinetics curves obtained from the bulk transmission and ATR experiments are similar but not identical. In each case, the β-sheet content of the protein aggregates was found to display two-stage kinetics. The initial phase of β-sheet growth rapidly saturated after ~400–700 s. This initial growth stage in the kinetics was also found to occur on similar timescales in both the ATR and bulk transmission studies.

DLS and ThT fluorescence studies performed at 60°C revealed that this first stage in the β-sheet kinetics was produced by the rapid formation of protein aggregates with an average radius of 13 ± 1 nm (see Fig. 3). The correspondence among the features observed in the FTIR data, the dynamic light-scattering experiments, and the ThT fluorescence measurements indicates that these initial aggregates contain significant amounts of intermolecular β-sheet (see Figs. 2 and 3). The presence of a measurable ThT intensity (above background levels) in the plateau region also suggests that repeat β-sheet folds are present in these aggregates (24). However, AFM images of the samples did not show the presence of any fibrils in the bulk solution or on the PS surfaces during this initial period of β-sheet growth (see *inset*, Fig. 2). Only small, less well-defined aggregates were observed with the AFM during this time period in both the bulk solution and PS surface experiments. The presence of nanoscale nonfibrillar aggregates has also been reported for other small polypeptides (25,26) during studies of fibril formation. We note at this point that great care must be taken in interpreting the AFM images shown in Fig. 2. The drying of protein solutions is often unreliable and can lead to different quantities of fibrils and other aggregates being

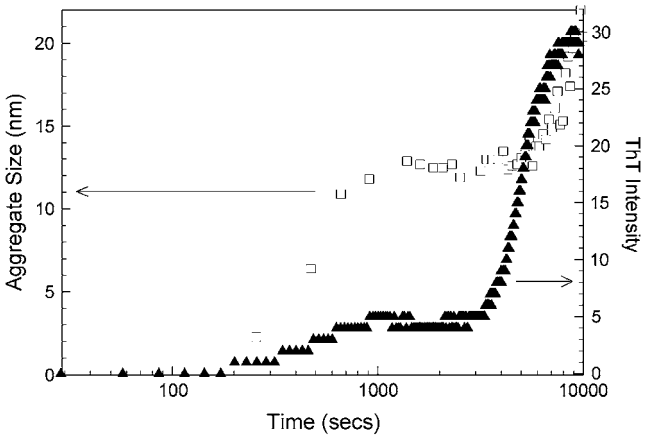

FIGURE 3 Dynamic light scattering (□, *left axis*) and ThT fluorescence studies (▲, *right axis*) of the aggregation on bovine pancreatic insulin. All data were collected at a temperature of 60°C and at pH 1.

observed on what should be identical samples. However, if sufficient AFM images are collected, this technique can be used to confirm the presence or absence of fibrils and to make qualitative comparisons between the morphologies of the aggregates that are formed.

The second, more rapid region of β-sheet formation was attributed to the growth of fibrils and was mirrored in both the ThT fluorescence and dynamic light-scattering studies. The presence of fibrils was confirmed by collecting AFM images of both PS surface-adsorbed and bulk-solution protein (see *inset*, Fig. 2). The onset of fibril formation was found to occur earlier at PS/water interfaces than in bulk solution, and the initial rates of fibril growth/β-sheet formation were found to be slower on the PS surfaces (as determined from the slopes of the curves in the *main panel* of Fig. 2). Qualitatively this indicates that fibril nucleus formation occurs faster on the PS surfaces than in bulk solution. The reduction in the growth rates associated with the β-sheet formation kinetics on the PS surfaces also indicates that the presence of the PS surface hinders the growth of insulin fibrils.

A consideration of the kinetics of the changes in the area of the amide II peak for the PS surface experiments (see *inset*, Fig. 2) indicates that a layer of protein was rapidly (within 15 s) adsorbed at the PS/water interface after the injection of BPI into the ATR sample cell. After this initial deposition, the amount of protein at the interface did not increase significantly until the onset of fibril growth. At this point, the amide II peak area increases along with the area of the β-sheet peak. This is likely to be caused by a combination of effects related to the addition of protein molecules to surface-nucleated fibrils (elongation) and the adsorption of bulk-nucleated fibrils on the PS surfaces (deposition). However, distinguishing between these two processes is not possible in the context of these experiments.

The final saturation point in the β-sheet absorbance kinetics was found to be similar for the PS surface and bulk solution at each temperature studied. At the point where the β-sheet kinetics saturated, the BPI solutions were found to form a viscous opaque gel. Cryo-scanning electron microscopy of these gels revealed that they contain a large tangled network of mature fibrils (data not shown).

In the bulk solution IR studies, the absorbance changes ($A(t)$) measured in the final stage of the β-sheet growth kinetics were found to follow an exponential rise of the form

$$A(t) = A_p + (A_o - A_p)\left(1 - \exp\left(-\frac{t - \tau_n}{\tau_a}\right)\right), \qquad (1)$$

where A_p and A_o are the absorbance values in the first plateau region and at saturation, respectively. The quantities τ_n and $1/\tau_a$ represent the fibril nucleation/lag time and growth rate, respectively. We note that care has to be taken in interpreting the parameter τ_a because this quantity contains information about both the elongation of existing fibrils and the nucleation of new fibrils that occurs during the late stages of β-sheet growth. Distinguishing between these two processes is not possible in the context of these experiments. However, τ_n is the time when fibrils are initially observed to form and represents a measure of the true nucleation/lag times in the system.

Fig. 4 shows semilogarithmic plots of the reduced absorbance ($1 - A(t)/A_o$) versus time for bulk solution protein (*panel a*) and PS surface-adsorbed protein (*panel b*) at a range of temperatures between 60°C and 80°C. In the ATR studies, multiple measurements were made at temperatures close to 65°C, 70°C, and 75°C to check reproducibility. However, the temperatures given in the caption in Fig. 4 are approximate values derived from the setting on the temperature controller and are not the actual temperature values. The actual temperature varied by as much as ±1°C from the temperature controller setting. The differences between the true measured temperature values and the approximate set-point values quoted in the figure caption

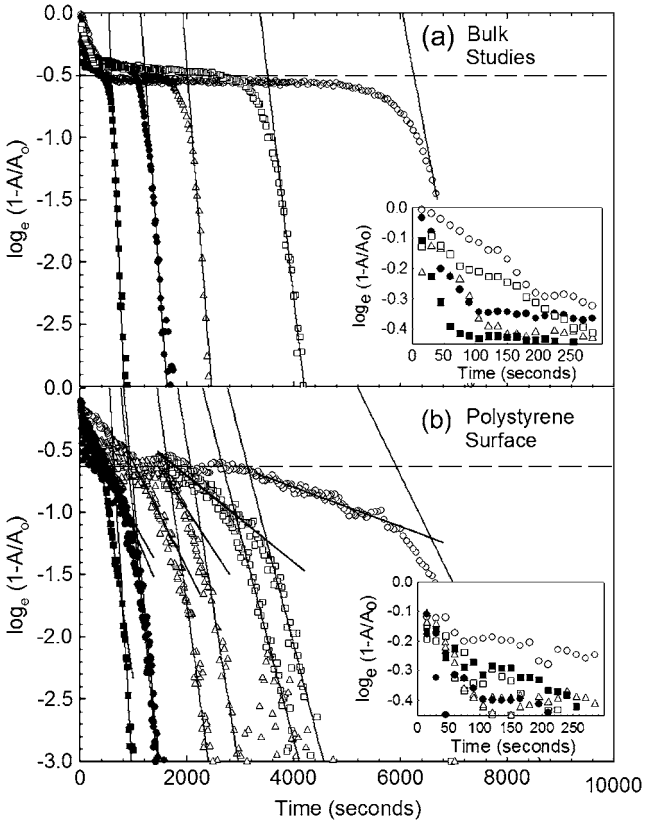

FIGURE 4 Semilogarithmic plots of the reduced β-sheet absorbance ($1 - A(t)/A_o$) of bovine pancreatic insulin versus time. Data are shown for the bulk aggregation kinetics (*top panel*) and for aggregation at a PS surface (*bottom panel*). In both cases data were collected at pH 1 and at temperatures close to 60°C (○), 65°C (□), 70°C (Δ), 75°C (●), and 80°C (■), respectively. All temperature values were measured with an uncertainty of ±1°C. The solid black lines show the fits used to determine the aggregation rates (see text). The horizontal dashed lines mark the position of the plateau region ($A = A_p$) that was used in determining the nucleation/lag time for fibril formation (see text).

account for the differences in kinetics that are observed between what should be identical data sets in the PS surface data shown in Fig. 4.

The experimental scatter that is observed in the bottom panel of Fig. 4 in the late stages of β-sheet formation is an artefact that occurs because the measured absorbance approaches the value A_0, and the corresponding value of $1 - A/A_0$ approaches the level of noise in the experiments. Taking the natural logarithm of the reduced absorbance therefore leads to this noise becoming clearly visible in the data as the value of A approaches its final value, A_0.

According to Eq. 1, plots of $\log_e (1 - A(t)/A_o)$ versus time similar to those shown in Fig. 4 should produce a straight line in the region corresponding to fibril growth with a slope that is equal to the aggregation rate, $1/\tau_a$. As can be seen in the top panel of this figure, this region is accurately fitted by a single straight line for the bulk data. In the case of the PS-adsorbed protein, two such linear regions exist (Fig. 4, *bottom panel*). The first slope is shallower than the slope observed for the bulk solution studies and occurs at earlier times. This slope was attributed to the formation of fibrils by insulin molecules that interact directly with the PS surface. AFM images of the PS surfaces taken during the period corresponding to the initial slope in the second stage of β-sheet growth showed evidence of a number of BPI fibrils at times when no bulk solution fibrils were observed (see *inset*, Fig. 2). The second slope in the PS surface data started at similar times and had comparable (but not identical) slopes to those observed in the bulk solution studies. This region was attributed to the bulk component of the signal acquired in the ATR experiments performed on the PS surfaces. These data are expected to show some features of the bulk solution response of the protein because the evanescent field used to probe the PS/water interface extends $\sim$1 μm into the solution. Although ATR is predominantly surface sensitive, the penetration depth of the evanescent field will extend beyond the thickness of any adsorbed protein layers and, as a result, will be sensitive to insulin molecules in bulk solution.

In each case, the slope of the linear regions was used to determine the aggregation/β-sheet growth rates ($1/\tau_a$) associated with the formation of BPI fibrils. The natural logarithm of the aggregation rate was then plotted against the inverse of temperature to produce Arrhenius plots for both bulk solution data and the PS surface data (see *top panel*, Fig. 5). The PS surface data shown in Fig. 5 are split into two components. The first corresponds to the bulk component of the aggregation measured in the ATR experiments, and the second corresponds to the true PS surface component of the data. This figure shows that the aggregation rates obtained from Fig. 4 are faster in bulk solution than on the PS surface. Moreover, the bulk solution aggregation rates appear to be faster than the bulk component of the aggregation kinetics measured using the ATR cell. This is discussed in more detail below.

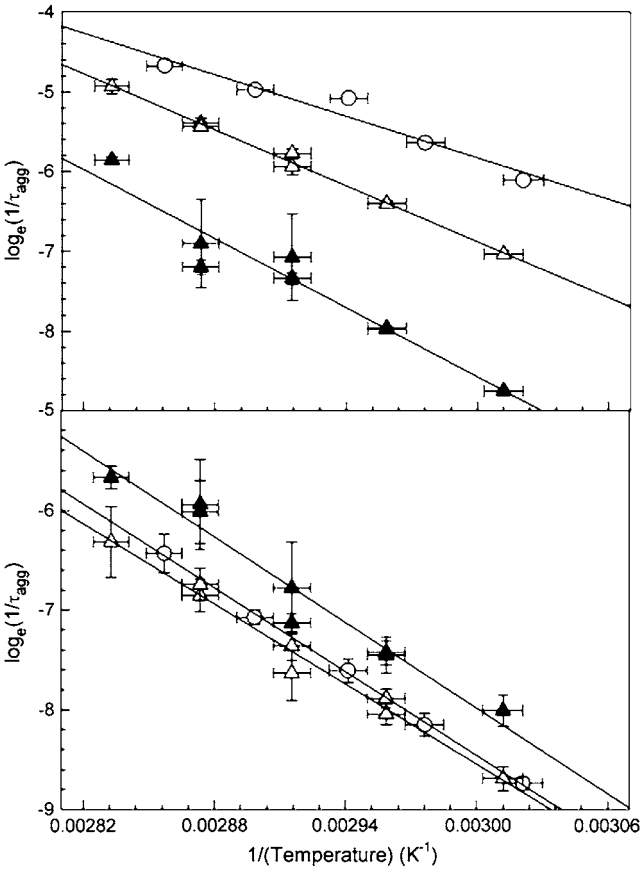

FIGURE 5 Arrhenius plots of the aggregation/fibrillization rates (*top panel*) and effective nucleation rates (*bottom panel*) of BPI at pH 1. Data are shown for bulk solution (○), the PS surface data (▲), and the bulk component of the PS surface data (Δ, see text). The solid lines represent fits to the form of Eq. 2.

The linear fits to the aggregation rate data shown in Fig. 5 were used to determine the energy barriers associated with fibril formation according to the Arrhenius equation

$$\log_e\left(\frac{1}{\tau_a}\right) = \log_e\left(\frac{1}{\tau_{a,o}}\right) - \frac{E_a}{RT}, \qquad (2)$$

where E_a is the energy barrier associated with fibril formation ($J \cdot mol^{-1}$), R is the molar gas constant ($J \cdot mol^{-1}K^{-1}$), T is the temperature (K), and $1/\tau_{a,o}$ is a characteristic attempt frequency associated with fibril growth (s^{-1}). At this point we note that the values of $1/\tau_a$ shown in Fig. 5 represent an average measure of the growth rates of all the aggregates in the system and not the individual fibril elongation rates. However, the amount of β-sheet formed in the system is expected to be directly proportional to the length of the fibrils formed. This means that under a given set of solution conditions, the aggregation/β-sheet formation rates shown in this figure will be related to the average fibril elongation rate by a simple numerical factor. However, the fact that E_a is derived from the temperature dependence of these scaled

aggregation rates means that E_a represents a measure of the true energy barrier for fibril growth.

The values obtained for the energy barrier, E_a from Fig. 5 are summarized in Table 1. The values shown are comparable to values that have been reported for insulin and proteins/peptides of comparable size under similar solution conditions (25,27). Table 1 clearly shows that the energy barrier associated with the growth of fibrils on PS surfaces is larger than the corresponding barrier associated with bulk solution fibril growth, within the limits of experimental uncertainty. This suggests that it is more difficult for fibrils to grow on hydrophobic PS surfaces than in bulk solution. The reason for this could be interpreted in a number of ways. The energy barriers presented in Table 1 represent a composite barrier that describes the change from the native solution state of the protein to an aggregated state. This energy barrier is therefore likely to include separate energy contributions related to differences in protein concentration and the colloidal and conformational stability of the protein molecules (15). The concentration and conformation of protein molecules adsorbed at the hydrophobic polymer surface and at the end of adsorbed fibrils are likely to differ from similar molecules in solution. These factors would be expected to alter the probabilities associated with the collision and sticking of two neighboring protein molecules. They would also affect the folding pathways associated with the attachment of protein molecules to the end of the growing fibril and would influence the corresponding contributions to the measured free energy barrier. The presence of charged protein molecules close to a dielectric material such as PS could also induce polarization charges in the polymer films that would alter the charge distribution around the tip of an adsorbed growing fibril. All of these factors could contribute to the observed differences in the aggregate/fibril growth barrier, but they are difficult to quantify in the context of this study.

It is also noteworthy that the energy barrier derived from the bulk component of the aggregation measured in the ATR experiments is larger than the energy barrier determined from bulk solution IR transmission measurements. As shown in Fig. 5 and Table 1, the aggregation rates and the energy barrier determined from the bulk component of the PS surface data fall in between those obtained for the ''true'' measured bulk and surface values. To determine the cause of this apparent discrepancy, a simple experiment was performed in which BPI was absorbed at a PS surface and the excess bulk solution protein was then flushed from the cell using the D_2O-based stock solutions. Measurement of the ATR spectra before and after flushing the cell showed that the measured absorbance from surface-adsorbed protein represented ~50% of the total measured signal. This accounts for the fact that the energy barrier and aggregation rates for the bulk component of the PS surface data appear to be weighted averages of the corresponding bulk and surface values.

TABLE 1 Energy barriers for fibril nucleation and growth

Energy barrier ($kJ \cdot mol^{-1}$)	Nucleation	Fibril growth
Bulk	117 ± 2	72 ± 10
Polystyrene (bulk component)	111 ± 6	97 ± 3
Polystyrene (surface component)	119 ± 11	120 ± 14

In addition to being used to determine the aggregation rates, the plots shown in Fig. 4 were also used to estimate the characteristic nucleation or lag times, τ_n, for the onset of fibril growth. This was done by determining the point of intersection of the fibril growth rate fit lines with the horizontal dashed lines used to define the plateau region in the kinetics (see Fig. 4). These nucleation times were then used to define an effective nucleation rate, $1/\tau_n$. The resulting nucleation rates are plotted on an Arrhenius diagram in the bottom panel of Fig. 5. The plots shown in Fig. 5 were used to extract the energy barriers (E_n) and attempt frequencies $1/\tau_{n,o}$ associated with the onset of fibril formation, using a similar procedure to that described for the fibril growth rates. The values of (E_n) that were obtained for the bulk solution and PS surface studies are summarized in Table 1. The energy barriers to fibril nucleation shown in Table 1 are comparable to (but smaller than) those observed for the aggregation of peptide chains of a similar size (28). As shown in Table 1, the nucleation barriers in all three cases are the same within the limits of experimental uncertainty. Initially, this may seem counterintuitive given that there are clear observable differences in the measured nucleation rates for the bulk and PS surface data sets (see Figs. 4 and 5). The presence of a hydrophobic interface might also be expected to cause the protein to unfold to expose more hydrophobic residues in the core of the insulin molecules to the PS surface. This would be expected to result in both a decrease in the enthalpy of interaction and an increase in the conformational entropy of the protein molecules (1) adsorbed at the PS/water interface. These combined factors would act to reduce the free energy barrier associated with the unfolding and subsequent aggregation of the protein. However, it is worth considering that the conformations adopted by the insulin molecules at the PS surfaces would not necessarily correspond to viable fibril-forming intermediate states. As a result, a surface-unfolded insulin molecule could experience a local conformational free energy barrier that is similar to that of a protein in bulk solution. The energy barrier associated with fibril nucleus formation would therefore not necessarily be altered significantly by forcing the protein to unfold at an interface.

Despite the fact that the fibril nucleation barriers are not significantly changed, Fig. 5 shows that the rates associated with the formation of fibril nuclei are increased by the presence of the PS surface. If the energy barriers associated with fibril nucleus formation remain unchanged, this suggests that the characteristic attempt frequencies associated with nucleus formation must be larger (see Eq. 2). One possible reason for this could be related to differences in the

concentration of protein molecules in the bulk and on the PS surfaces. In the ATR experiments, the PS surfaces were rapidly coated (within 15 s) with a surface excess of insulin. This resulted in a larger local protein concentration at the surface than in bulk solution. The localization of a ''dense'' layer of protein at the PS surface would therefore increase the probability of two insulin molecules coming into contact and would result in a corresponding increase in the attempt frequency associated with the formation of viable fibril nuclei.

Regardless of the mechanism that is responsible for the accelerated formation of fibril nuclei, this experimental observation has some potentially far-reaching implications with regard to the toxicology of high-surface-area nanoscale materials. Fibril precursors have recently been implicated as being the toxic species in a number of amyloid-related diseases (29). As these experiments show, the presence of artificial surfaces such as the model PS surfaces studied causes the more rapid formation of these fibril precursors or nuclei. This means that great care must be taken to assess the full toxicological impact of new nanoscale diagnostic and therapeutic agents before they are released on to the market.

It is not clear if the smaller aggregates formed in the initial stages of aggregation play a role in the formation of fibrils. If the formation of fibril nuclei was influenced by the presence of these smaller aggregates, then we would expect to observe a correspondence between the temperature dependence of the fibril nucleation rates and that of the rates associated with the formation of these smaller aggregates. A comparison of the rates associated with β-sheet formation during small aggregate formation (see *insets*, Fig. 4) shows that there are factors of 4 and 10 difference between the lowest and highest temperatures studied for the bulk solution and PS surface experiments, respectively. The difference in the fibril nucleation rates at the two temperature extremes studied corresponds to a factor of 10 in the values determined from Fig. 5. This would seem to suggest that there is some correlation between the formation of these smaller aggregates and the onset of fibril nucleation. However, the data presented in the insets of Fig. 4 contain significant amounts of scatter, and more detailed analysis of these results would be unreasonable. More detailed studies of the early-stage kinetics of formation of these small aggregates would be required to determine if they are linked to fibril nucleation.

The timescales associated with both the nucleation and growth of fibrils shown in Fig. 4 are similar to those reported for insulin under similar solution conditions (30). We note that the study performed by Krebs and co-workers (30) deals mainly with the study of amyloid spherulites of insulin and not directly with insulin fibrils. However, because the formation of amyloid spherulites involves the growth of fibrillar material around an ''amorphous'' protein core, we would expect the timescales associated with the formation of amyloid spherulites to be comparable to those measured in fibril growth studies performed under similar solution conditions. It is also worth remarking that no amyloid spherulites were observed during the experiments described in the study presented here. Crossed-polarizer light microscopy, SEM, and AFM were used to look for the presence of spherulites. The characteristic micrometer-sized birefringent structures that are associated with the formation of amyloid spherulites were not observed in any of the samples studied and could be observed only when foreign nucleating agents (such as small colloidal particles) or undissolved protein were added to the solutions.

At the temperatures studied, the fibril nucleation and growth rates (see Fig. 5) have values that vary between $\sim 1 \times 10^{-4}\ s^{-1}$ and $\sim 2 \times 10^{-2}\ s^{-1}$. The characteristic time associated with the folding of a β-sheet ''hairpin'' structure has been reported for peptide chains that are comparable in size to an insulin molecule (25,31). These studies showed that the time associated with the folding of a β-hairpin structure for an isolated peptide chain is of the order of ~ 20 μs, but the timescales associated with formation of intermolecular β-sheet structures during aggregation can be significantly longer (~ 2 ms). These timescales correspond to rates of $\sim 5 \times 10^{4}\ s^{-1}$ and $\sim 500\ s^{-1}$, respectively. The aggregation/fibril growth rates measured in this study are up to 10^{8} times smaller than the rates associated with the formation of intermolecular β-sheet. This suggests that conformational changes alone are not sufficient to account for the aggregation rates measured here and that the growth rates of insulin fibrils at the pH values and salt concentrations studied are also mediated by other factors such as colloidal stability (15). This is not surprising when consideration is given to the fact that the isoelectric point of insulin occurs at 5.3 (32) and the pI of the solutions studied is 1. Under such solution conditions, each insulin molecule would be expected to carry a net charge of $\sim 9.6 \times 10^{-19}$ C ($+6e$) (1,17). This would result in the formation of charged double layers (33) around the insulin molecules that would repel neighboring proteins and reduce the associated aggregation rates.

In each case the characteristic attempt frequency ($1/\tau_o$) was typically found to lie in the range 10^{12}–$10^{14}\ s^{-1}$. This is comparable to the high-temperature relaxation rate of a simple liquid ($\sim 10^{13}\ s^{-1}$) and represents a reasonable upper bound for the attempt frequency (25). This is because both fibril nucleation and growth are expected to involve the translation of molecules from the surrounding solution environment to the tip of the growing fibril. However, a more detailed analysis of the attempt frequencies would be unrealistic because these values are obtained by extrapolating the aggregate growth rates by over 10 orders of magnitude.

CONCLUSIONS

A method has been presented for determining the rates of aggregation and the energy barriers associated with insulin fibril nucleation and growth in bulk solution and at model PS surfaces. These experiments showed that the presence of

hydrophobic PS surfaces promoted the nucleation of fibrils but did not affect the size of the fibril nucleation barrier (within error). The PS interface did, however, increase the energy barrier associated with the growth/elongation of insulin fibrils. These observations were briefly explained in terms of the differences in conformational and colloidal stability of the proteins in solution and on surfaces as well as differences associated with protein concentration effects and the mobility of the insulin molecules. The method described in this work involves the use of well-established IR spectroscopy–based protein characterization methods, and we anticipate that this technique could also be used to study aggregation in other protein/surface systems.

We thank Dr. Sno Stolnick (School of Pharmacy) for providing access to the dynamic light-scattering apparatus. We are grateful to the University of Nottingham's Interdisciplinary Doctoral Training Centre in Nanotechnology for providing access to a project studentship for this work. We also thank the Engineering and Physical Sciences Research Council, the Nuffield Foundation, and the University of Nottingham for providing funding.

REFERENCES

1. Sharp, J. S., J. A. Forrest, and R. A. L. Jones. 2002. Surface denaturation and amyloid fibril formation of insulin at model lipid-water interfaces. *Biochemistry*. 41:15810–15819.
2. Adams, S., A. M. Higgins, and R. A. L. Jones. 2002. Surface-mediated folding and misfolding of proteins at lipid/water interfaces. *Langmuir*. 18:4854–4861.
3. Zhu, M., P. O. Souillac, C. Ionescu-Zanetti, S. A. Carter, and A. L. Fink. 2002. Surface-catalyzed amyloid fibril formation. *J. Biol. Chem.* 277:50914–50922.
4. Sluzky, V., J. A. Tamada, A. M. Klibanov, and R. Langer. 1991. Kinetics of insulin aggregation in aqueous solutions upon agitation in the presence of hydrophobic surfaces. *Proc. Natl. Acad. Sci. USA*. 88:9377–9381.
5. Dobson, C. M. 2003. Protein folding and misfolding. *Nature*. 426:884–890.
6. Ahmad, A., I. S. Millet, S. Doniach, V. N. Uversky, and A. L. Fink. 2003. Partially folded intermediates in insulin fibillation. *Biochemistry*. 42:11404–11416.
7. Chamberlain, A. K., C. E. MacPhee, J. Zurdo, L. A. Morozova-Roche, H. Allen, O. Hill, C. M. Dobson, and J. J. Davis. 2000. Ultrastructural organization of amyloid fibrils by atomic force microscopy. *Biophysics*. 79:3282–3293.
8. Žerovnik, E. 2002. Amyloid fibril formation: proposed mechanisms and relevance to conformational disease. *Eur. J. Biochem*. 269:3362–3371.
9. Dowling A., R. Clift, N. Grobert, D. Hutton, R. Oliver, O. O'Neill, J. Pethica, N. Pidgeon, J. Porritt, J. Ryan, A. Seaton, S. Tendler, M. Welland, and R. Whatmore. 2004. Nanoscience and Nanotechnologies: Opportunites and Uncertainties. The Royal Society & The Royal Academy of Engineering, UK.
10. Vaseashta, A., and D. Dimova-Malinovska. 2005. Nanostructured and nanoscale devices and detectors. *Sci. Tech. Adv. Mater*. 6:312–318.
11. Tischer, B. K., D. Schumacher, M. Beer, J. Beyer, J. P. Teifke, K. Osterrieder, K. Wink, V. Zelnik, F. Fehler, and N. Osterrieder. 2002. A DNA vaccine containing an infectious Marek's disease virus genome can confer protection against tumorigenic Marek's disease in chickens. *J. Gen. Virol*. 83:2367–2376.
12. Chi, E. Y., S. Krishnan, T. W. Randolph, and J. F. 2003. Carpenter. Physical stability of proteins in aqueous solution: mechanism and driving forces in nonnative protein aggregation. *Pharm. Res*. 20:1325–1336.
13. Garriques, L. N., S. Frokjaer, J. F. Carpenter, and J. Brange. 2002. The effect of mutations on the structure of insulin fibrils studied by Fourier transform infrared (FTIR) spectroscopy and electron microscopy. *J. Pharm. Sci*. 91:2473–2480.
14. Ahmad, A., V. N. Uversky, D. Hong, and A. L. Fink. 2005. Early events in the fibrillation of monomeric insulin. *J. Biol. Chem*. 280: 42669–42675.
15. Brange, J., L. Andersen, E. D. Laursen, G. Meyn, and E. Rasmussen. 1997. Toward understanding insulin fibrillation. *J. Pharm. Sci*. 86: 517–525.
16. Raman, B., T. Ban, K. Yamaguchi, M. Sakai, T. Kawai, H. Naiki, and Y. Goto. 2005. Metal ion-dependent effects of clioquinol on the fibril growth of an amyloid β-peptide. *J. Biol. Chem*. 280:16157–16162.
17. Nielsen, L., S. Frokjaer, J. F. Carpenter, and J. Brange. 2001. Studies of the structure of insulin fibrils by Fourier transform infrared (FTIR) spectroscopy and electron microscopy. *J. Pharm. Sci*. 90:29–37.
18. Jiménez, J. L., E. J. Nettleton, M. Bouchard, C. V. Robinson, C. M. Dobson, and H. Saibil. 2002. The protofilament structure of insulin amyloid fibrils. *Proc. Natl. Acad. Sci*. 99:9196–9201.
19. Bouchard, M., J. Zurdo, E. J. Nettleton, C. M. Dobson, and C.V. Robinson. 2000. Formation of insulin amyloid fibrils followed by FTIR simultaneously with CD and electron microscopy. *Protein Sci*. 9:1960–1967.
20. Krebs, M. R. H., C. MacPhee, A. Miller, I. Dunlop, C. M. Dobson, and A. M. Donald. 2004. The formation of spherulites by amyloid fibrils of bovine insulin. *Proc. Natl. Acad. Sci. USA*. 101:14420–14424.
21. Hiramatsu, H., and T. Kitagawa. 2005. FTIR approaches on amyloid fibril structure. *Biochim. Biophys. Acta*. 1753:100–107.
22. Dzwolak W., R. Ravindra, J. Lendermann, and R. Winter. 2003. Aggregation of bovine insulin probed by DSC/PPC calorimetry and FTIR spectroscopy. *Biochemistry*. 42:11347–11355.
23. Dzwolak W., S. Grudzielanek, V. Smirnovas, R. Ravindra, C. Nicolini, R. Jansen, A. Loksztejn, S. Porowski, and R. Winter. 2005. Ethanol-perturbed amyloidogenic self-assembly of insulin: looking for origins of amyloid strains. *Biochemistry*. 44:8948–8958.
24. Krebs, M. R. H., E. H. C. Bromley, and A. M. Donald. 2005. The binding of thioflavin-T to amyloid fibrils: localisation and implications. *J. Struct. Biol*. 149:30–37.
25. Kusumoto, Y., A. Lomakin, D. B. Teplow, and G. B. Benedek. 1998. Temperature dependence of amyloid β-protein fibrillization. *Proc. Natl. Acad, Sci. USA*. 95:12277–12282.
26. Podestà, A., G. Tiana, P. Milani, and M. Manno. 2006. Early events in insulin fibrillization studied by time-lapse atomic force microscopy. *Biophys. J*. 90:589–597.
27. Mauro, M., E. F. Craparo, A. Podestà, D. Bulone, R. Carrotta, V. Martorana, G. Tiana, and P. L. San Biago. 2007. Kinetics of different processes in human insulin amyloid formation. *J. Mol. Biol*. 366:258–274.
28. Sabaté R., M. Gallardo, and J. Estelrich. 2005. Temperature dependence of the nucleation constant rate in β-amyloid fibrillogenesis. *Int. J. Bio. Macromol*. 35:9–13.
29. Kayed, R., E. Head, J. L. Thompson, T. M. McIntire, S. C. Milton, C. W. Cotman, and C. G. Glabe. 2006. Common structure of soluble amyloid oligomers implies common mechanism of pathogenesis. *Science*. 300:486–489.
30. Krebs, M. R. H., E. H. C. Bromley, S. S. Rogers, and A. M. Donald. 2005. The mechanism of amyloid spherulite formation by bovine insulin. *Biophys. J*. 88:2013–2021.
31. Muñoz, V., R. Ghirlando, F. J. Blanco, G. S. Jas, J. Hofrichter, and W. A. Eaton. 2006. Folding and aggregation kinetics of a β-hairpin. *Biochemistry*. 45:7023–7035.
32. Conway-Jacobs, A., and L. M. Lewin. 1971. Isoelectric focusing in acrylamide gels: use of amphoteric dyes as internal markers for determination of isoelectric points. *Anal. Biochem*. 43:394–400.
33. Israelachvili, J. 1991. Intermolecular and Surface Forces, 2nd ed. Academic Press, Oxford, UK.